Colalongo *et al*. *Microstructures* 2024;4:2024044
**DOI:** 10.20517/microstructures.2024.19

**Microstructures**

**Research Article**

**Open Access**

# Imaging inter - and intra-particle features in crystalline cathode materials for Li-ion batteries using nano-focused beam techniques at 4th generation synchrotron sources

**Mattia Colalongo[1,2#], Nikita Vostrov[1#], Isaac Martens[1], Edoardo Zatterin[1], Marie-Ingrid Richard[1,3], Francois Cadiou[1], Quentin Jacquet[4], Jakub Drnec[1], Steven J. Leake[1], Tanja Kallio[3], Xiaobo Zhu[5], Sandrine Lyonnard[4], Tobias Schulli[1]**

[1]The European Synchrotron ESRF, Grenoble 38000, France.
[2]Department of Chemistry and Material Science, School of Chemical Engineering, Aalto University, Espoo 02150, Finland.
[3]University Grenoble Alpes, CEA Grenoble, IRIG, MEM, NRS, Grenoble 38000, France.
[4]University Grenoble Alpes, CEA, CNRS, Grenoble INP, IRIG, SyMMES, Grenoble 38000, France.
[5]College of Materials Science and Engineering, Changsha University of Science and Technology, Changsha 410114, Hunan, China.
[#]Authors contributed equally.

**Correspondence to:** Dr. Tobias Schulli, European Synchrotron Radiation Facility, 71 Avenue des Martyrs, Grenoble 38000, France. E-mail: schulli@esrf.fr

**How to cite this article:** Colalongo M, Vostrov N, Martens I, Zatterin E, Richard MI, Cadiou F, Jacquet Q, Drnec J, Leake SJ, Kallio T, Zhu X, Lyonnard S, Schulli T. *Microstructures* 2024;4:2024044. http://dx.doi.org/10.20517/microstructures.2024.19

**Received:** 29 Feb 2024 **First Decision:** 28 Apr 2024 **Revised:** 14 May 2024 **Accepted:** 28 May 2024 **Published:** 24 Jul 2024

**Academic Editor:** Shaobo Cheng, Shanqing Zhang **Copy Editor:** Fangling Lan **Production Editor:** Fangling Lan

## Abstract

The necessity of mapping crystal defects in battery materials after synthesis is crucial in understanding heterogeneity within a single crystal domain and among particles to develop superior crystal quality materials. Numerous imaging techniques have been developed over the past years to study these materials at the nanoscale. However, most of them use electron beams which demand many hours of sample preparation, and they are incompatible with the investigation of batteries under realistic working conditions. Techniques such as Scanning X-ray Diffraction Imaging (Scanning X-ray Diffraction Microscopy) or Bragg Coherent Diffraction Imaging are increasingly available on the latest generation synchrotron sources. Their progressive deployment will allow for a standardized method for imaging crystal lattice imperfections such as lattice tilt and strain in individual particles without any prior sample preparation. In this paper, we exploited Scanning X-ray Diffraction Microscopy to probe the strain variation in single crystals and polycrystalline particles and Bragg Coherent Diffraction Imaging to reconstruct the volume of a single crystal particle. Presented case studies were performed on particles of different active cathode materials ($LiNi_{0.6}Mn_{0.2}Co_{0.2}O_2$, $LiNiO_2$ and $LiMn_{1.5}Ni_{0.5}O_4$); however, these techniques can also be employed on other battery components for a more holistic structural understanding of used materials and (de)lithiation dynamics on the microscale.

**Keywords:** Li-ion batteries, SXDM, NMC, LNO, LMNO, BCDI

## INTRODUCTION

Large-scale electrification of the global economy requires cheap, efficient, and durable energy storage. The decreasing cost of high-performance lithium (Li)-ion batteries has generated widespread interest for applications that require far longer lifespans than typical consumer electronics. A wide range of characterization techniques are employed to systematically study and improve modern battery materials. Powder X-ray diffraction (PXRD) remains the most common method used to evaluate crystal quality in different battery components and in particular in cathode materials, while also being applicable for *operando* measurements for investigation of their structural evolution. However, this method yields, by definition, averaged information over a large number of crystals.

Structural heterogeneities present in primary particles such as lithiation irregularities, defects, grain boundaries and lattice misorientations are practically invisible during powder diffraction measurements. Such imperfections of the crystal lattice can be formed in the particles either during the synthesis or as a result of long-term cycling and are considered to be an important aspect affecting the electrochemical performance and stability of the material[1,2]. High variation of lattice quality among different particles in the cathode can also explain the reported discrepancy of electrochemical results between different studies. This underlines the importance of careful crystal quality assessment after synthesis and its monitoring during long-term cycling on different scales for a more holistic understanding of battery systems. However, directly measuring device aging performance of different active materials is extremely slow and expensive; therefore, heuristic tools that can predict aging performance from microstructure would be a valuable asset.

Structural differences among various particles, e.g., the inter-particle lithiation heterogeneity, also remain mostly unaccounted for in powder diffraction techniques and require the use of specialized techniques. For example, such studies of inter-particle structural heterogeneity using X-ray diffraction (XRD) and spectroscopy techniques can uncover previously unaccounted features of phase transformations[3] and correlate crystallographic heterogeneity with the structural degradation among different particles[2].

There are several microscopy techniques that allow for imaging of battery materials with a single crystal spatial resolution. X-ray microscopy techniques such as Scanning Transmission X-ray Microscopy (STXM) and micro-X-ray fluorescence (XFM) both give elemental information, in particular Li-ion concentration[4–6]. Optical microscopy techniques such as optical interferometric scattering microscopy (iSCAT) offer similar chemical information with comparable spatial resolution[7]. Chemically resolved spatial information is especially important to study the lithiation pathways and Li-ion heterogeneity across different particles. However, chemical mapping data obtained using these methods gives only indirect information about the local crystal structure. In addition, *operando* measurements with the aforementioned techniques require specialized cells optimized for specific experiments that can be not representative in terms of electrochemical behavior and can introduce some experimental challenges such as the need for a vacuum environment or samples with extremely dispersed crystals[5,6].

Recently, Laue micro-diffraction technique was used to effectively study the crystal defects in cathode materials[8]. This technique could be an invaluable tool for quality control of battery material since it allows the identification of a wide range of different defect types and quantification of their amount in the sample. However, to the best of our knowledge, successful *operando* Laue diffraction experiments have not yet been reported. Electron Backscatter Diffraction (EBSD) opens up a possibility for measurements of crystal orientation which is valuable for studying the structure of the secondary particles in polycrystalline cathode materials[9]. Never-

theless, the angular resolution does not allow the study of fine misorientation of crystal structure in primary single crystals.

Single particle strain imaging inside battery crystals has been performed before using atomic resolution transmission electron microscopy (TEM) or Bragg Coherent Diffraction Imaging (BCDI)[1,10–12]. Steady improvements in the strain resolution of phase-sensitive, coherent techniques such as BCDI offer interesting opportunities to study defective cathode structures. However, such techniques face fundamental barriers in measuring industrially relevant particles of several microns in size, since they are limited by the coherence length of the X-ray beam[13]. While TEM allows significantly better spatial resolution than these novel X-ray techniques, it faces even steeper restrictions in terms of field of view, crystallite thickness and has only limited *operando* capabilities. The present article highlights the importance of multiparticle and single particle imaging of cathode materials on the example of Scanning X-ray Diffraction Microscopy (SXDM) and BCDI. Going beyond conventional powder diffraction investigations, these methods are able to reveal unique structural information on single and multiparticle scales. SXDM is a flexible technique that exploits nanosize beams[14] and allows monitoring of both inter- and intra-particle structural heterogeneity for polycrystalline and single crystal materials. The BCDI technique uses a highly coherent X-ray beam[15] to probe 3D strain fields with high-resolution inside primary particles. These techniques require a highly brilliant X-ray source and are thus essentially exploitable on 3rd or 4th generation synchrotron sources. A leading instrument in this field is the beamline ID01 at the European Synchrotron Radiation Facility (ESRF)[16]. Both of these techniques are available for users with developed pipelines for measurements and data analysis. This opens up an opportunity for systematic studies of battery materials that focus on understanding the influence of variations in synthesis, composition, morphology, *etc*. on their electrochemical performance and stability. Wide flexibility of the ID01 beamline also allows for integration of different experimental setups and techniques[15,16] that facilitate a holistic understanding of battery material structure on various scales ranging from tens of nanometers to hundreds of micrometers. We have previously shown how SXDM can reveal a broad variety of defects inside nominally single crystal $LiNi_{0.6}Mn_{0.2}Co_{0.2}O_2$ (NMC-622) at high spatial resolution[17] and successfully followed the phase transition inside a $LiMn_{1.5}Ni_{0.5}O_4$ (LMNO) particle[12]. In this work, we present a set of case studies on $LiNiO_2$ (LNO), NMC622 and LMNO cathode materials investigated using SXDM and BCDI. These examples highlight the possibility of probing lattice quality with an unprecedented resolution on different scales ranging from single crystals up to an ensemble of polycrystalline particles. In addition, flexibility of these techniques lifts most of prior sample preparation requirements and simplifies the measurements in *operando* conditions.

## METHODS AND MATERIALS

### SXDM principles

SXDM is an imaging technique where a nanofocused X-ray beam is rastered across a sample, measuring diffraction in Bragg reflection geometry from each position of a real space map [Figure 1A][12,14]. In a SXDM experiment, the diffraction signal from the particles in the Bragg condition in the sample is collected by a 2D detector at the $2\theta$ of the Bragg reflection of interest. To obtain the full 3D information of the diffracted peak in reciprocal space, the sample is rotated around an axis perpendicular to the beam, varying its incidence angle [Figure 1A]. In this way, a set of 2D slices of reciprocal space in the vicinity of the studied Bragg reflection is obtained for each position on the sample [Figure 1B]. This set of data collected is what is called a rocking curve scan. An example of a rocking curve on a particle is presented in Supplementary Figure 1. By merging the rocking curve 2D slices, it is possible to obtain the intensity distribution of the Bragg reflection in a 3D volume of the reciprocal space for each *XY* sample position. In a 3D-SXDM map, the position and shape of the Bragg reflections contained in each (*XY*) scanned position can be analyzed to obtain local diffraction information. To streamline the analysis and data interpretation, a simple Center of Mass (COM) fitting is used to determine the coordinates of the Bragg reflection (and therefore the magnitude and the direction of the local scattering vector $Q_{local}$). More detailed analysis of the diffracted intensity is possible by fitting the reflection

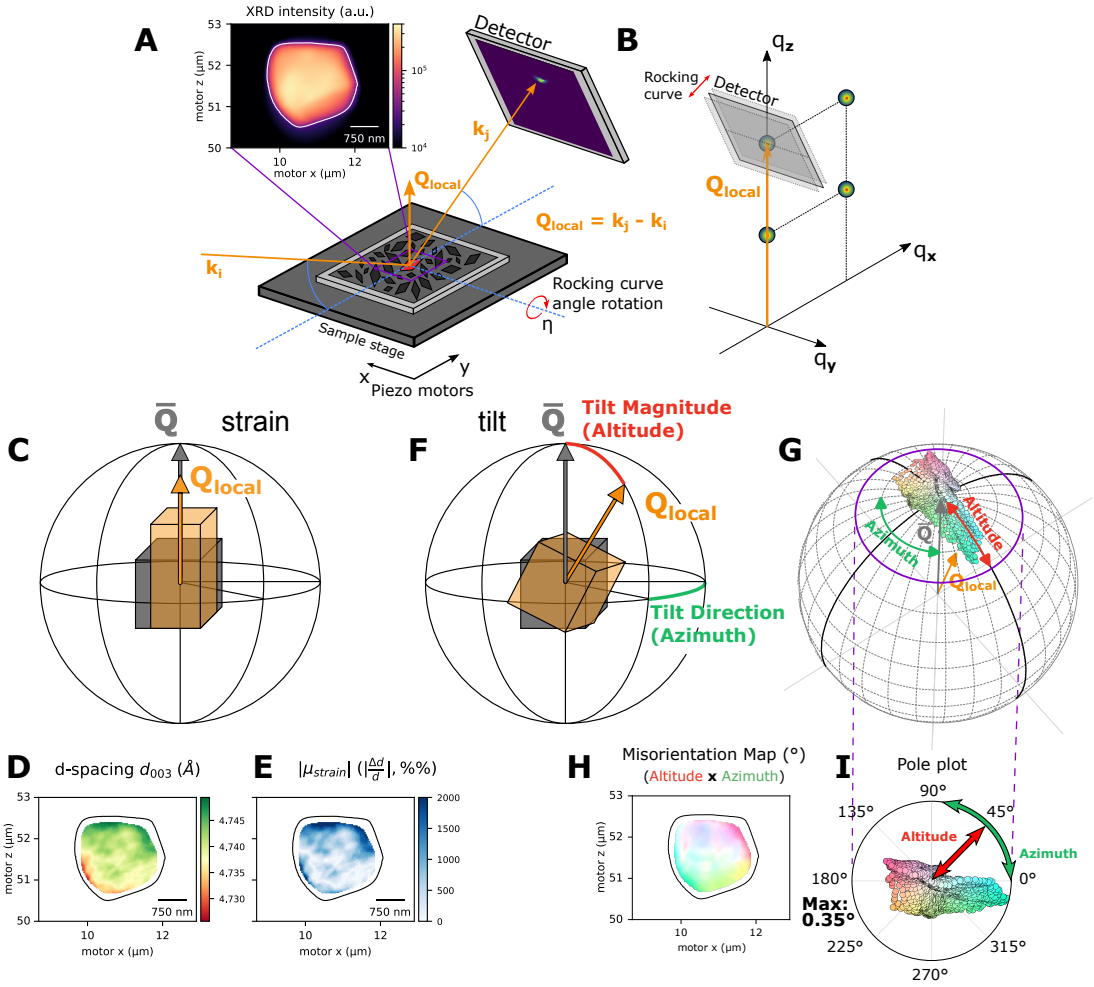


**Figure 1.** Scanning X-ray Diffraction Microscopy (SXDM) experimental schematics (A). A nanofocused beam (with wave-vector $k_i$) is rastered across the sample (using piezo motors x and y) imaging crystals found in Bragg conditions in the scanned area. For each step of the map local scattering vector, $Q_{local}$ is measured which is defined as the difference between $k_i$ and $k_f$, incident and scattered wave vectors, respectively. It corresponds to the studied Bragg reflection and contains local diffraction data of the illuminated portion of the crystal. Maps are obtained at distinct rocking curve angles $\eta$ to probe the 3D volume of the reciprocal space. The slices measured at each rocking curve angle by the 2D detector define the studied volume in the reciprocal space, which contains the Bragg reflection of the particle (B). SXDM is sensitive to the magnitude variation of the $Q_{local}$ scattering vector (orange) relative to the averaged scattering vector ($\overline{Q}$ (gray)) across the measured particle (C). These local variations can be visualized as maps of absolute d-spacing (D) or "strain" relative to average d-spacing of the particle (E). Rotation of $Q_{local}$ vector in the reciprocal space due to lattice mosaicity/misorientation can also be detected (F). The direction of $Q_{local}$ vector can be expressed in spherical coordinates as tilt magnitude (Altitude) and tilt direction (Azimuth) (G) (Tilt magnitude is exaggerated for clarity). Lattice mosaicity can also be visualized on the map of the same scanned area (H) by color coding the altitude and azimuth values with saturation and hue, respectively (I).

with a Gaussian function and calculating the peak width along each axis of the reciprocal space.

The obtained local scattering vector is extremely sensitive to the local changes in d-spacing (the magnitude of the $Q_{local}$ presented in Figure 1C). Strain inside the particle can be displayed either as the variation in d-spacing (see Figure 1D), or, more conveniently, as the local deviation of the d-spacing from the mean value of the whole crystal ($\frac{\Delta d}{d} \cdot 10^6$) (see Figure 1E).

Another unique information that can be obtained by investigating the local scattering vector is the local crystallographic misorientation/mosaicity of the measured planes (rotation of the $Q_{local}$ shown in Figure 1F). Small rotations, tilts, bending, and geometric distortions of different domains inside the crystal are collectively referred to as mosaicity. While strain measurement is a more mature methodology due to the possibility of its

extraction from conventional diffraction patterns, measurements of crystal mosaicity and orientation distributions at the nanoscale are still in their infancy. A variety of approaches have emerged to probe this additional dimension of microstructural complexity with the necessary precision[18–21], but a robust understanding of the origins and influence of mosaicity has not been established for battery materials yet.

As can be seen in Figure 1G, the direction and magnitude of these tilts can be expressed with azimuth and altitude angles in a spherical coordinate system, the main axis of which points along the average Q-vector of the particle ($\overline{Q}$), and mapped directly onto the crystal [Figure 1H]. The hue represents the direction of the tilt (azimuth), while the saturation intensity of the color conveys the magnitude of the local tilt *vs.* the average orientation of the whole crystal (altitude). The local rotation of the crystal lattice can either be directly mapped onto the crystal structure [Figure 1H], or visualized in the form of a pole figure, where the direction and magnitude of the tilt are calculated in spherical coordinates [Figure 1G and I]. By investigating the shape of the Bragg reflection along different axes ($Q_x$,$Q_y$ and $Q_z$) at each point of the maps, it is possible to determine the degree of heterogeneity of aforementioned parameters along the illuminated volume at each position on the crystal Supplementary Figures 2 and 3.

This relatively new technique[14] has been recently used to image the strain and defect structure of battery cathode microcrystals[8,21–23]. In addition to excellent sensitivity towards crystalline microstructure, nanodiffraction has two advantages over soft X-rays[5] and electron beam[24] spectromicroscopy for battery materials. Firstly, penetration through sample environment up to several centimeters thick[25], providing compatibility with industrially relevant materials and secondly, potentially lower beam-induced damage[26] as the beam energy can be arbitrarily tuned to reduce absorption phenomena. Furthermore, spectroscopic imaging, which follows transition metals through their oxidation state, cannot differentiate ordered/disordered phases and crystalline strain due to $Li^+$ dishomogeneities.

SXDM is frequently used for thin films where the sample thickness can be negligible[27–30], but in this study, the 2D projection of a 3D particle is measured. Therefore, the diffraction signal is averaged through the "depth" of the crystal, projected along the incident beam direction. This introduces some amount of ambiguity into the acquired maps of the particle that requires additional scrutiny during their interpretation. This can be resolved by obtaining a 3D reconstruction of the particle and strain fields with BCDI technique which will be discussed later.

### SXDM data analysis

Python scripts utilizing the XSOCS and SXDM libraries developed at ESRF[31,32] were used to analyze the data. Conversion of the diffracted intensity to reciprocal space was done by "binning" the diffracted intensity data in each voxel of an array and applying a $2 \times 2$ median filter. The size of the array was calculated in each case to match the resolution determined by the detector orientation, its distance from the sample and rocking curve step. The 3D fitting of the center of mass of a Bragg peak was used to determine the direction and the length of local Q-space vectors. The images were masked to exclude pixels with less than 20% of the maximum diffraction intensity.

### SXDM measurements

SXDM measurements were performed at the ID01 beamline of the ESRF. Fresnel Zone Plates are used to focus the X-ray beam down to nanometer size (50-120 nm depending on the beam energy). For *ex situ* SXDM experiments, no special sample preparation is required. However, it is preferable, especially for cathodes with small particle size (< 500 nm), to minimize the number of the crystals in the path of the beam since only one particle should satisfy the Bragg condition for a certain position of the detector to efficiently isolate the diffraction data and keep the scanned particle in the center of rotation. This can be achieved, for example, by using thinner cathode films. The sample (in this case, a piece of a cathode film) is glued or taped to a magnetic holder and

placed in the focal point to achieve the highest resolution. *Operando* experiments require an electrochemical cell that allows for X-ray measurements in reflection geometry[12,33] (e.g., the Leriche cell[34] or *operando* cells from EL-CELL. The design[16] and acquisition strategy[14] have been discussed in detail elsewhere. For each $x$, $y$ raster position, a 2D diffraction pattern is collected, but to fully sample the whole Bragg peak in reciprocal space, rocking curves were performed over a range covering several times the full width at half maximum (FWHM) of the Bragg peak. A monochromatic beam with an X-ray energy of 8.33 keV (1.48 Å wavelength) was focused onto the sample with a Fresnel zone plate of 300 micrometers in diameter and an outermost zone width of 30 nm leading to a spot size of about ~40 nm. Diffraction patterns were collected with a 512 × 512 Maxipix detector with an exposure time of at least 10 ms per pixel.

To overcome eventual sample drifting due to center of rotation misalignment during the rocking curve scan, the particle is linearly re-positioned at each rocking angle to account for all eccentricity contributions. An example of shift correction is reported in Supplementary Figure 4. COM calculations per pixel were evaluated over a selected region of interest (see Supplementary Figure 5).

### BCDI principles

BCDI is a powerful technique that allows the visualization of, in 3D, lattice strain and displacement fields in crystallites[15,35–38]. It is based on the fundamental principle of mathematical equivalence of diffraction phenomenon to Fourier transformation. Upon certain conditions such as full coherence of the X-ray beam, full illumination of the particle and sufficient diffracted signal oversampling, it is possible to fully reconstruct the shape, and the lattice deviations inside, of the crystal by essentially performing inverse Fourier transform of the diffraction signal. Here, iterative algorithms are employed to reliably retrieve the phase of the signal that is lost after detection of the diffraction from a crystal[39].

### BCDI measurements

Similar to SXDM, BCDI does not require any sample preparation for *ex situ* experiments and requires the same type of electrochemical *operando* cells. However, unlike SXDM, BCDI requires a fully coherent X-ray beam and correct oversampling in both the detector plane and along the rocking curve. This implies positioning the detector at a distance that fulfills the oversampling condition (oversampling greater than 2, i.e., at least 2 pixels per fringe, the Nyquist limit), and ensuring that the steps of the rocking curve also meet the oversampling requirement. The sample was mounted on a high-precision (~1 nm) XYZ-stage that is installed on the diffractometer of the ID01 beamline. The beam energy was set to 13 keV and focused down to a ~ 1 μm beam using a set of Beryllium compound refractive lenses. The diffracted signal was recorded with a Maxipix photon-counting detector (pixel size of 55 × 55 μm) positioned on the detector arm at a distance of 1.4 m. We measured the 004 LMNO Bragg reflection in three dimensions by rotating the particle around its Bragg angle ($\theta$) over 0.4°.

### Materials

Commercial SC-NMC622 was provided by MSE Supplies (batch N. 29520B1). LNO pristine electrodes with a loading of 3 mAh/cm$^2$ were provided by BASF and consist of 94 wt% LNO (BASF), 3 wt% C65 carbon black (TIMCAL) and 3 wt% Solef5130 polyvinylidene fluoride (PVDF, Solvay). Disordered LMNO cathode material was prepared by polymer-assisted sol-gel method which was described in detail in our earlier work[12]. The active material was made into electrodes using a doctor blade onto Al foil (99.6%, 15 μm) thick, Guangdong Canrd Ltd), with an ink composition of 85 wt% LMNO, 10% conductive carbon, and 5% PVDF (Solef PVDF 5130/1001, Solvay) binder with N-methyl pyrrolidone (NMP) serving as the solvent.

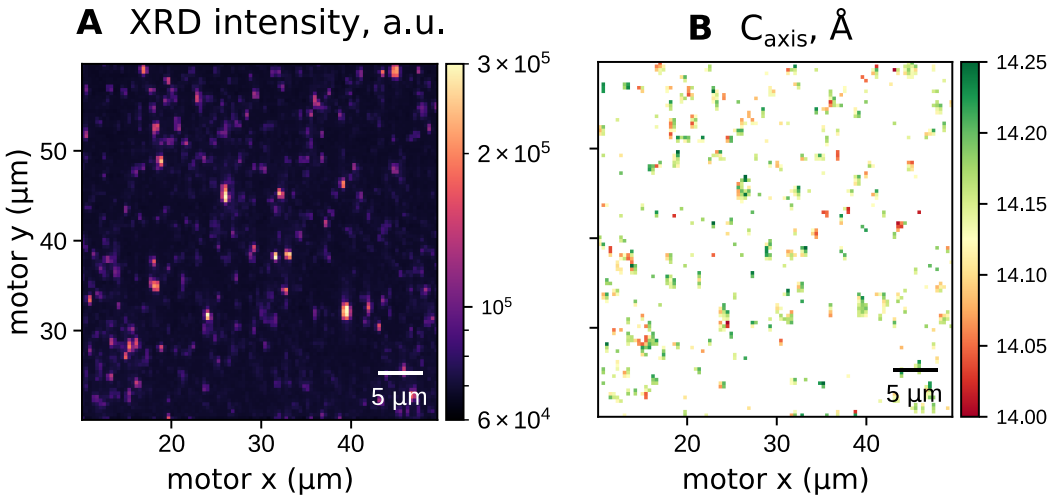


**Figure 2.** 40 × 40 µm SXDM map of LNO polycrystalline pristine powder. Pixel resolution ~ 400 nm. XRD intensity of multiple single crystals in Bragg condition (A). $c_{axis}$ lattice parameter extracted by fitting the Bragg peak Center of Mass (COM) of each single pixel within the collected map (B).

## RESULTS

The current SXDM setup on the ID01 beamline at ESRF [16] allows the study of lattice heterogeneity on various scales that are relevant for the battery material research. Several instrumental parameters can be adjusted to satisfy possible experimental requirements in field of view, strain sensitivity, time resolution, *etc*. These parameters include the beam size which is controlled by the choice of the focusing optics, the focusing distance, the detector distance which determines the resolution and the field of view in reciprocal space, the size of the scanned region, and the rocking curves step size and range which are related to the reciprocal space resolution. This flexibility in the beamline setup opens up a possibility for a wide range of experiments on materials with different morphologies and allows automatic and dynamic switching between different modes of operation during an experiment [33].

In this paper, we demonstrate the unique range of possibilities using SXDM and BCDI techniques available at the ID01 beamline. SXDM provides local 2D maps of the strain and tilt of the measured planes at different scales. The size of the mapped regions can vary from 40 × 40 to 100 × 100 µm with the spatial resolution defined by size of the beam (30-120 nm). We will first present high Field of View (FoV) scans of multiple single crystals in polycrystalline LNO particles, followed by more in-depth high-resolution measurements of lattice structure inside single-crystal NMC622 (SC-NMC622) cathode material.

BCDI, on the other hand, provides a 3D strain map of a single particle. This technique achieves a spatial resolution smaller than the beam size through iterative reconstruction algorithms. The BCDI technique is limited to isolated crystalline nano- and micro-scale objects. For the demonstration of BCDI capabilities, we will present full 3D BCDI reconstruction of a morphology and strain distribution of LMNO crystals.

### SXDM on polycrystalline materials

Study of inter-particle structural heterogeneity is of great interest due to particle-by-particle charging kinetics path dependencies and particle-by-particle differences in Li-ion concentration. From an electrode engineering perspective, a heterogeneous reaction across a population of particles could lead to an increased current density in a fraction of active particles and thus be a reason for accelerated degradation of that specific cathode material portion, especially when fast C-rates are employed [3,40]. Moreover, the redistribution of lithium ions between particles was suggested to be a reason for hysteresis between the charge and discharge voltages [41].

To understand the intra- and inter-particle heterogeneity of polycrystalline electrodes, we performed various SXDM maps for different spatial resolutions on pristine LNO cathode material embedded in a conventional electrode film that shows particles with a polycrystalline nature as seen on the Scanning Electron Microscopy (SEM) images [Supplementary Figure 6]. XRD analysis is presented in Supplementary Figure 7.

The first map of 40 × 40 µm with a resolution of 400 nm per pixel (see the diffraction intensity map in Figure 2A) shows that multiple crystals satisfy the Bragg condition for the 003 reflection. A map of $d_{003}$-spacing values corresponding to each position on the same map is presented in Figure 2B. Considering the direct relation of the $c_{axis}$ lattice constant to the Li-ion concentration, this map reveals sample-wide structural heterogeneity likely caused by uneven Li-ion distribution among different crystals in the sample. Therefore, the advantage of SXDM over the conventional PXRD lies in its potential to retrieve positional information in real space of the diffracting crystals. Furthermore, in addition to the d-spacing or $c_{axis}$ distribution, per pixel in the 2D map, SXDM is also sensitive to local angular orientation and lattice distortion. D-spacing distribution maps come in handy for the exploration of inter/intra particle heterogeneities. However, differentiating primary particle domains within a cluster of pixels might be challenging. In Figure 3A, a smaller portion of the map is taken into account where two clusters of particles are diffracting. To recognize whether two pixels belong to the same crystallite or not, with this specific resolution, it is necessary to additionally inspect the corresponding Bragg peak in reciprocal space per individual pixel.

By investigating neighboring positions in the pixel cluster on the right of Figure 3A (highlighted by black and white crosses), we can see only a minimal change in Bragg reflection position in the slices of the reciprocal space in Figure 3B. This likely indicates that the diffraction signal produced by these two pixels is coming from one single crystal. Yet, the d-spacing variation between the black and white cross pixels is 14.043 and 14.057 Å, respectively, suggesting intra-particle heterogeneity. The lattice tilt misorientation at the white and black crosses in Figure 3A is rather significant (~ 0.18°), as shown in Supplementary Figure 8. Such deformation of the single crystals was observed before and can be a sign of high defect concentration due to degradation or issues during synthesis[17,42,43]. However, for a more detailed insight into the low angle lattice misorientations in a single crystal, it is better to probe the internal gradients at sub-100 nm resolution, as will be demonstrated later.

By looking at the particle cluster to the left side of the map in Figure 3A and selecting two pixels close to each other (highlighted by red and blue crosses), it is evident that, in addition to the small $c_{axis}$ value variation, the Bragg peak position in $Q_y$ is considerably different as displayed in two bottom slices of the reciprocal space in Figure 3B. The d-spacing values for the red and blue crossed pixels are 14.136 and 14.147 Å, respectively, whereas the tilt magnitude is ~ 15.06°, as reported in the polar plot in Supplementary Figure 8. Although both clusters show d-spacing heterogeneity, for the left cluster, such a large variation in diffraction signal position along $Q_y$, as shown in Figure 3B, could be caused by two highly misoriented grains of a polycrystalline particle with the diffraction signal from both of them hitting the field of view of the detector. The other explanation is related to the 2D projection limitation of SXDM and suggests the presence of a second crystallite at a different depth in the sample, while appearing close on the measured 2D map. In both cases, inter-particle heterogeneity can be investigated, in particular the lithiation state of different single crystals across the sample. For a more detailed study, the ambiguity mentioned before can be resolved with a higher resolution map which, in addition, can be useful for investigating grain boundaries in polycrystalline materials which are expected to be a limiting factor for ionic conductivity inside of secondary particles and can be a reason of failure in the form of cracking and pulverization of cathode particles[44–47].

In Figure 4, we present the scan of a 2 × 2 µm area in an LNO electrode using 50 rocking steps. As before, we were able to detect multiple crystals in Bragg condition which are well separated in reciprocal space but now with much higher spatial resolution. This type of q-space Bragg peak segregation ultimately allows us to select

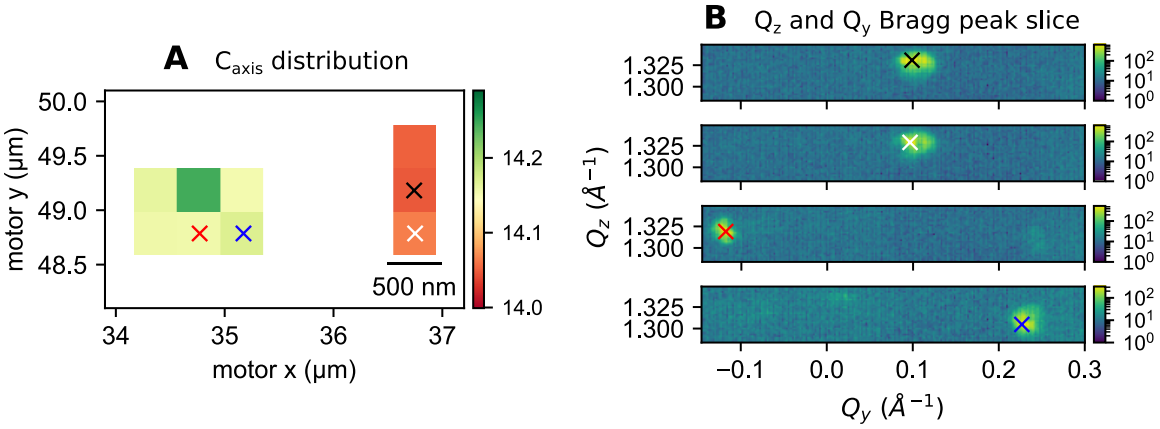


**Figure 3.** (A) a zoomed in portion of the 40 × 40 µm map. The map shows a clear cluster of particles for each pixel. (B) is reported the relative Bragg peak in the $Q_z$ and $Q_y$ slice for the selected pixel

regions of interest related to separate crystals in real space. The diffraction intensity of LNO particles shown in the blue and red box in Figure 4A and their relative $c_{axis}$ value variation in Figure 4B can be separately identified by selecting a specific region of interest in reciprocal space, as reported in Figure 4C. In fact, within the collected reciprocal space volume, a cluster of LNO crystals of similar size and a larger single crystal were found. Interestingly, the small cluster of crystals, highlighted in the blue box, shows a homogeneous intra-particle d-spacing distribution and a heterogeneous inter-particle distribution. As the 003 peak position of this layered cathode material is sensitive to the $Li^+$ occupancy within transition metal slabs where any variation of $Li^+$ concentration would change the d-spacing values of the unit cell[48], it comes as no surprise to identify possible crystallites with relatively lower Li-ion content, especially after the lithiation process upon synthesis. The larger crystal highlighted in the red box in Figure 4 shows instead an internal gradient within the same crystal domain. This intriguing gradient observed, albeit limited on a 2D projection, indicates a heterogeneous Li-ion distribution inside the single crystal domain. The additional advantage of SXDM on the larger LNO crystal lies in the possibility of also retrieving internal mosaicity information. This is evident in Figure 4D; the larger crystal exhibits two distinctive sub-domains within a single particle. Furthermore, the maximum tilt extent shown in Figure 4E is ~0.7°. Large tilt values and the presence of clear subdomains are usually ascribed to the existence of a large number of crystal defects[12] typical of fused crystals. These two examples underline the feasibility of obtaining a statistical relevant map, achieved through a wide field of view, and a higher resolution map, enabling exploration of intra-particle features within single crystals. Moreover, a combination of both maps is required to differentiate the details of Li-ion content heterogeneities arising from either inherent material structure or cycling-induced inter/intra-particle variations with respect to the sample average behavior.

### SXDM of single-crystalline materials

Single-crystal $LiNi_xMn_yCo_zO_2$ (SC-NMCs) are promising positive electrode materials because of their superb resistance to cracking even at high voltages, avoiding electrolyte penetration along grain boundaries, increasing their stability over cycling[49]. As explained earlier, the application of SXDM provides access to distinctive internal structural features within the single crystal domain. In this case study, pristine SC-NMC622 crystals were probed by means of scanning nanobeam diffraction. SEM reveals an average particle size of 2 µm (see Supplementary Figure 9) and all the reflections in PXRD (see Supplementary Figure 10) matched the expected layered structure, with no relevant impurity. To be representative of the bulk sample, two different particles of 2-3 µm and an average $c_{axis}$ parameter of ~ 14.22 Å were measured. Particle size, $c_{axis}$ distribution and $\overline{c}$ (average $c_{axis}$ value over the particle) for both particles are reported in Supplementary Figure 11. Equivalent to the LNO sample, the vicinity of the 003 reflection was probed for the NMC622 sample in order to probe the $c_{axis}$ of the

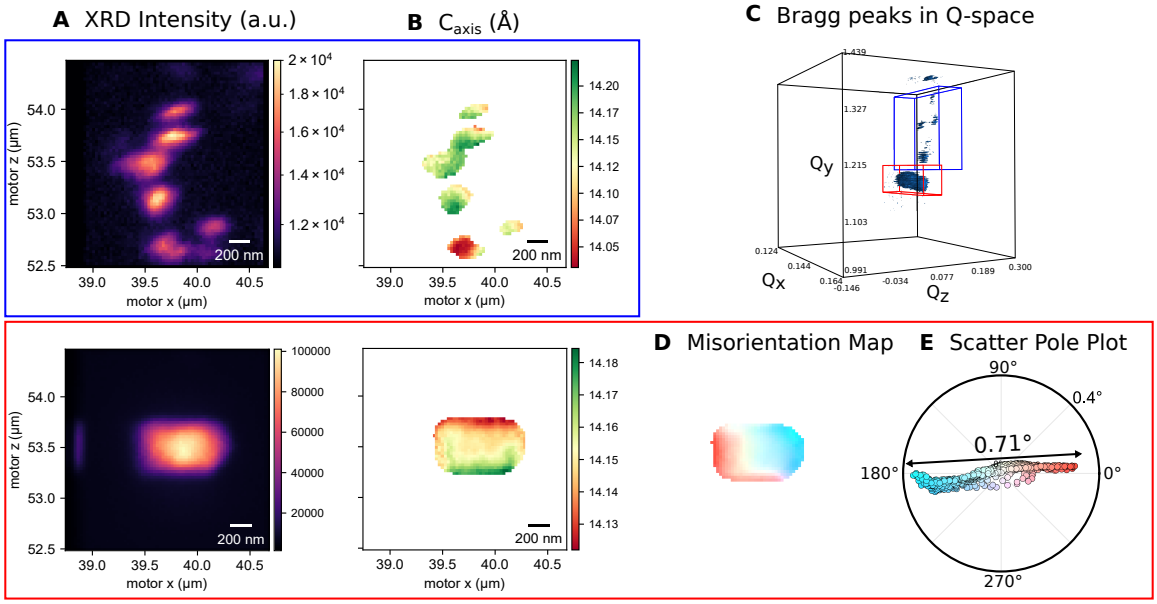


**Figure 4.** (A) XRD intensity of a cluster of LNO crystals (top) and a larger single crystal (bottom). (B) Respective d-spacing map along the $c_{axis}$ of the unit cell.( C) Visualization of the crystals Bragg peaks in reciprocal space. (D) Misorientation map of the LNO large crystal. (E) Pixel distribution of misorientation map in the polar scatter plot.

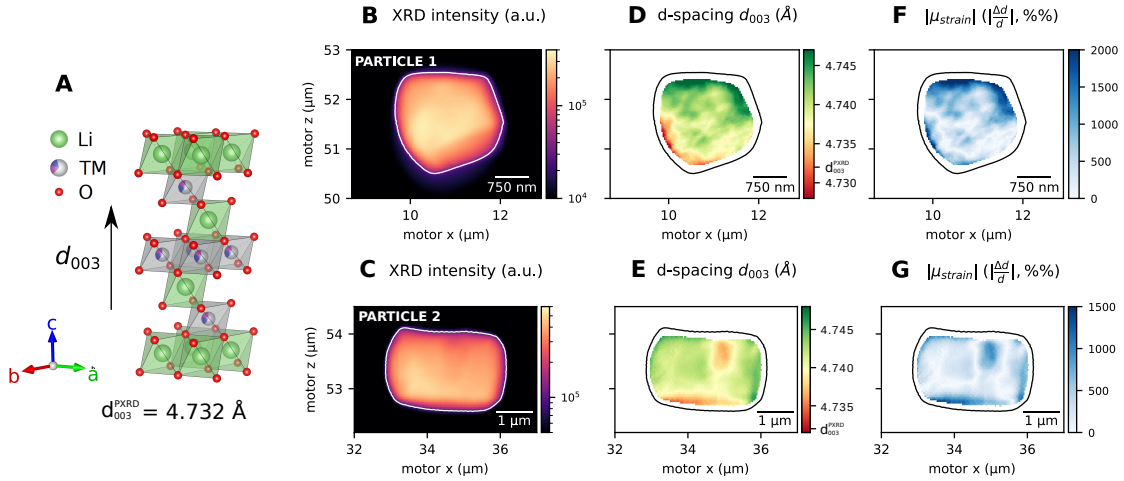


**Figure 5.** Scanning X-ray nano-diffraction microscopy of NMC-622 cathode single crystal. NMC-622 crystal structure, showing the inter-layer distance ($d_{003}$) between transition metal and lithium slabs probed by the diffraction imaging (A). Diffraction intensity map for two single crystal particles (B and C), extracted d-spacing map (D and E), absolute $\mu_{strain}$ variation map defined as $|\Delta d/d| \cdot 10^6$ (F and G).

unit cell (see Figure 5A). The variation of the $c_{axis}$ is often related to Li-ion occupancy variation and Ni/Li cation mixing within the crystal structure. A noteworthy result is related to the particle's shape; although the obtained images are a 2D projection of the crystal, the faceted nature of each single crystal is clearly recognizable in the diffracted intensity images in Figure 5B and C. Both particles appear to possess morphological characteristics indicative of high-quality crystals. However, SXDM probes nanoscale crystallographic variations in the bulk of the particle. Both particles show *intra-particle* $c_{axis}$ lattice parameter heterogeneities, as presented in their respective d-spacing maps in Figure 5D and E. Plotting d-spacing maps as difference from an averaged value ($\bar{d}$) is visually more informative, as it enables the detection of compressive and tensile strain within the scanned crystal region. However, we are mostly interested in the absolute d-spacing variation from its average value, which reveals areas with higher strain within the single crystal region as reported in Figure 5F and G.

Despite the internal heterogeneity for both particles dictated by the d-spacing value variation, Particle 1 shows an overall higher $|\mu_{strain}|$ compared to Particle 2. In general, as a result of a stress relaxation mechanism, high strain values are linked to a higher concentration of defects. Furthermore, tilt magnitude and tilt direction are a symptom of stress relaxation mechanism due to high concentration of defects and crystal mosaicity, respectively. As shown in Figure 6A and B, both SC-NMC622 particles show higher values of tilt magnitude close to the crystal facets or particle edges. To visualize the crystal mosaicity, Figure 6C and D represents tilt direction maps for Particles 1 and 2 allowing us to spot multiple crystal domains within the whole particle; in fact, the left side of Particle 2 has pixels with an azimuth > 0 (colored in lightblue, blue and violet), whereas the right side pixels of the map have azimuth < 0 (colored in green, yellow and red) suggesting at least two main crystal sub-domains from left to right. Particle 1, instead, owns a more complex directional tilt map; in fact, we are able to identify three major sub-domains colored in lightblue/blue, yellow/green and purple/red. However, the information on tilt direction alone might be misleading as the direction map needs to be combined with the magnitude map to better understand the crystal mosaicity. As shown in Figure 6E and F, Particle 1 possesses rather small bulk mosaicity, whereas it appears highly defective and tilted on the edges. Particle 2, on the contrary, shows two large tilt domains from left to right from the bulk all along to the edges, as if composed of two distinct crystal domains. Also, here, the largest saturation values ascribed to the tilt magnitude are found close to the particle edge. It is rather normal to observe multiple crystal domains in single crystal cathode materials knowing the synthesis process of the individual crystals where high calcination temperatures are used to fuse multiple crystals together.

The scattering vector rotation at each pixel of the particle (which corresponds to the local lattice misorientation) can be better visualized in Figure 6G and H where the direction and the magnitude of the tilt are represented in a scatter pole plot. Interestingly, the maximum tilt extension of Particle 1 (0.54°) is larger than the one of Particle 2 (0.26°). Even though, to a certain extent, they both present mosaicity indicating crystal sub-domains, Particle 1 exhibits an overall larger crystal distortion, especially closer to the particle edges. Cation mixing and dislocations along with sub-domain distortions are often ascribed to the formation of oxygen vacancies upon single crystal growth[50]. The required temperatures needed for the growth of single crystals often result in lithium evaporation, as $Li_2O$, and oxygen instability in the host structure[51], leading to a defective lattice. To improve the crystal quality of these materials, the mosaicity degree expressed by the maximum tilt extension should be smaller as compared to previously studied spinel-like materials[12] in order to reduce the possibility of crack formation upon cycling and improve the life span of single crystal cathode materials. It is important to note that SXDM yields 2D projection images of a 3D volume; therefore, the information per pixel is the average value along the beam path across the entire particle which can somewhat hinder the data interpretation. Nevertheless, we can observe high defect concentration in both particles, especially close to their edges.

### Single-crystalline BCDI

BCDI is another nanodiffraction technique that gained traction recently in the field of battery research[39,52]. By illuminating the whole crystal with a highly coherent X-ray beam available at ID01, it is possible to extract a full 3D reconstruction of both the internal distribution of strain and the electron density of the particle[16,52]. This is done by applying iterative reconstruction algorithms[53,54]. The full 3D reconstruction of a crystal allows for a noticeably easier data interpretation compared to the projection-summed 2D maps obtained with SXDM. This, however, comes at the cost of significantly more complicated data analysis procedures where a successful reconstruction is not always guaranteed for strongly strained particles with higher defect concentrations or deformations. Indeed, when employing the BCDI technique, consideration of multiple parameters becomes essential. For instance, highly strained particles may experience overlapping fringe features along a diffracting streak, resulting in an information loss for the phase retrieval process. Moreover, the larger the crystal, the more the fringes in reciprocal space will get closer together. While the latter issue can be mitigated by increasing the detector distance from the sample stage to ensure the appropriate pixel resolution, such adjustments are often constrained by the geometry of the beamline. For these reasons, better candidates are often crystals

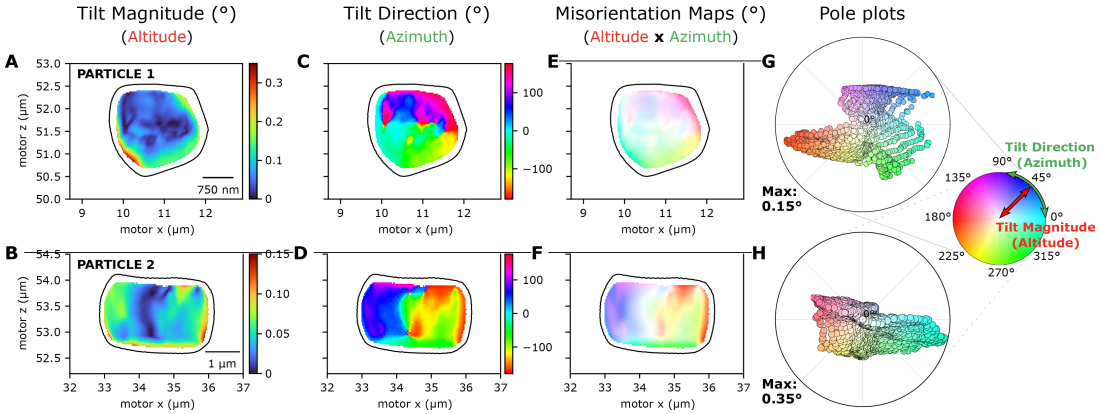


**Figure 6.** Scanning X-ray nanodiffraction microscopy of NMC622 cathode single crystal. Tilt Magnitude of crystal deviation from mean direction (altitude) (A and B). Local distortion in orientation of lattice *vs.* mean direction (azimuth) (C and D). Crystal misorientation map (Direction · Magnitude) (E and F). Pixel distribution of Misorientation Map projected on the 2D scatter polar plot (G and H)

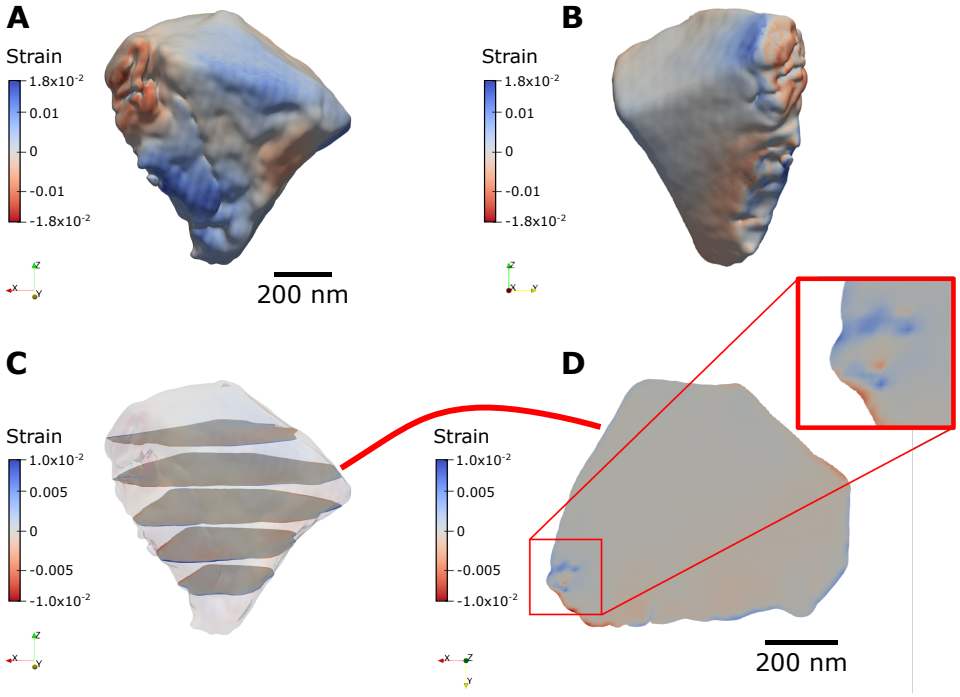


**Figure 7.** BCDI reconstruction of an LMNO particle (A and B). Several slices of the particle representing the strain distribution along the [004] direction inside the particle (C). One of the slices that includes strain heterogeneity (zoomed in) in the crystal (D).

within the range of 200-1,000 nm in size and not highly strained. The first size condition would be satisfied by the population of LNO crystals, yet they are highly strained. A perfect candidate for BCDI is the previously studied LMNO single crystals[17] which show lower misorientation magnitude and lower strain compared to layered cathode materials. Displayed in both Figure 7A and B is a reconstructed LMNO particle from the 004 Bragg reflection measured *ex situ* (see Methods and Materials). The particle size is about 800 nm. Very interestingly, facets are observed over the particle and can be indexed as {111} facets. Higher strain on the surface of the particle is consistent with SXDM data. BCDI allows the observation and identification of strain heterogeneities or defects within the crystal lattice. Specifically, as shown in Figure 7C, it is possible to visualize 2D cross-sections from the 3D strain field map, ultimately accessing defects distribution at a specific particle

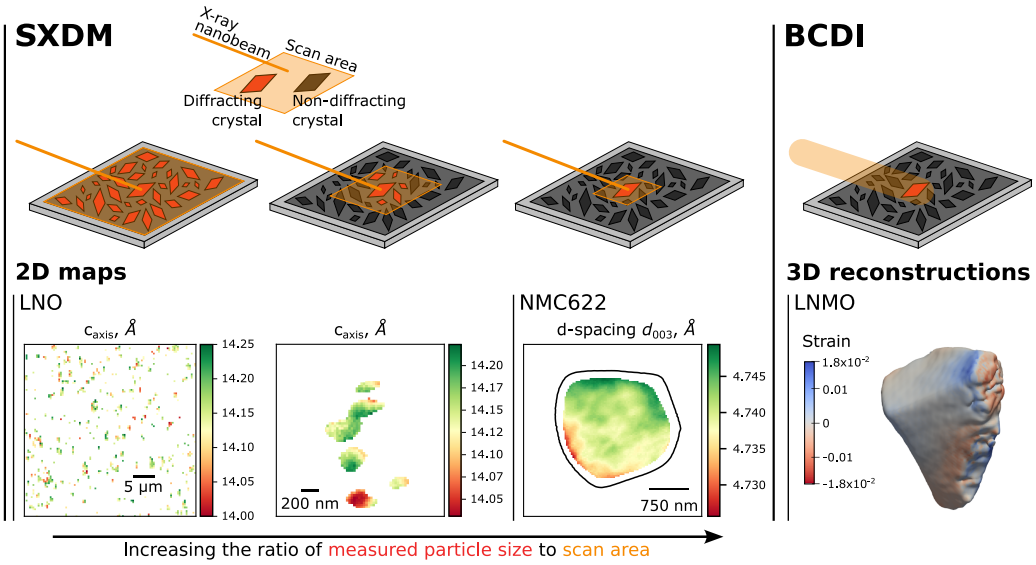


**Figure 8.** A schematic overview of the presented techniques including different operation modes of Scanning Diffraction X-ray Microscopy (SXDM) (A-C) (with varying ratios of the measured area to the scanned area) and Bragg Coherent Diffraction Imaging (BCDI) (D). SXDM produces 2D maps of structural heterogeneities (E-G) while BCDI allows the retrieval of a 3D reconstruction of the particle with strain fields inside of it.

position as observed in Figure 7D. The heterogeneous strain distribution and defects and their influence on the delithiation pathways can be followed *operando* during cycling of the particle. Contrary to SXDM for which the spatial resolution is limited to the beam size, here, the resolution is estimated to be 20 nm[3].

## CONCLUSIONS

In this study, we highlight a variety of case studies where techniques available at the ID01 beamline of ESRF can unveil microstructural variations in various cathode materials with different particle morphologies. An advanced technique such as SXDM allowed the discernment of inter and intra-particle heterogeneity for a polycrystalline case study at varying map resolutions. Furthermore, the use of SXDM proved to be particularly effective in identifying internal crystal features for highly strained and defective single crystals. Notably, the main advantage of this technique lies in its ability to map entire crystal domains with exceptionally high-resolution and minimal sample preparation, indicating its potential as a tool for predicting the impact of crystal defects on cathode performance, consequently guiding their development upon synthesis. However, building structure-activity relationships in materials with a large quantity and diversity of defects is still challenging, because the individual contributions of all structural motifs are convoluted, and the features overlap in images. This main limitation of SXDM ascribed to the impossibility of visually retrieving the whole 3D strain field map can be addressed by means of the BCDI technique. As demonstrated in this study, heterogeneous strain distribution within a crystal can be resolved. Additionally, by navigating within the crystal volume slices, it is possible to pinpoint individual defects in the strain field map. Figure 8 presents an overview of SXDM and BCDI experimental setups and the type of retrievable data that can be useful for holistic understanding of battery materials on different scales. The widespread utilization of these techniques for *operando* studies is crucial for comprehending the evolution of defects, thereby offering unprecedented insights into the development of superior cathode materials.

## DECLARATIONS

### Acknowledgments

The authors thank Hamid Djazouli for expert technical support, Ewen Bellec for helping during the data inter-

pretation process and Vladimir Kutyrin for 3D data visualization

### Authors' contributions

Designed the experiment: Jacquet Q, Lyonnard S, Cadiou F, Martens I, Vostrov N, Colalongo M
Performed the measurements: Colalongo M, Vostrov N, Martens I, Richard MI, Cadiou F
Processed the experimental data and performed the data analysis: Colalongo M, Vostrov N, Zatterin E, Richard MI
Drafted the manuscript and designed the figures: Vostrov N, Colalongo M
Provided the samples to measure: Cadiou F, Jacquet Q, Zhu X, Lyonnard S
Provided access to ID01 inhouse beamtime: Schulli T, Leake SJ
Supervised the project: Schulli T
Contributed to the manuscript editing, review and scientific discussion: Colalongo M, Vostrov N, Martens I, Zatterin E, Richard MI, Cadiou F, Jacquet Q, Drnec J, Leake SJ, Kallio T, Zhu X, Lyonnard S, Schulli T

### Availability of data and materials

The data that support the findings of this study are available from the authors, Colalongo M, Vostrov N upon reasonable request.

### Financial support and sponsorship

This work was supported by the European Research Council (ERC) under the European Union's Horizon 2020 research and innovation program (Grant agreement numbers 814106 (TEESMAT) and 818823 (CARINE)). We thank BIGMAP for providing LNO cathode: EU H2020 Research and Innovation Program project BIGMAP under grant agreement No. 957189; and the hub for beamtime: Beamtime at the ESRF was granted within the Battery Pilot Hub MA4929 "Multi-scale Multitechniques investigations of Li-ion batteries: towards a European Battery Hub".

### Conflicts of interest

All authors declared that there are no conflicts of interest.

### Ethical approval and consent to participate

Not applicable.

### Consent for publication

Not applicable.

### Copyright



## REFERENCES

1. Harris SJ, Lu P. Effects of inhomogeneities-nanoscale to mesoscale-on the durability of Li-ion batteries. *J Phys Chem C* 2013;117:6481-92. DOI
2. Finegan DP, Vamvakeros A, Tan C, et al. Spatial quantification of dynamic inter and intra particle crystallographic heterogeneities within lithium ion electrodes. *Nat Commun* 2020;11:631. DOI
3. Park J, Zhao H, Kang SD, et al. Fictitious phase separation in Li layered oxides driven by electro-autocatalysis. *Nat Mater* 2021;20:991-99. DOI
4. Wang L, Wang J, Zuo P. Probing battery electrochemistry with in operando synchrotron X-ray imaging techniques. *Small Methods* 2018;2:1700293. DOI
5. Lim J, Li Y, Alsem DH, et al. Origin and hysteresis of lithium compositional spatiodynamics within battery primary particles. *Science* 2016;353:566-71. DOI
6. Ohmer N, Fenk B, Samuelis D, et al. Phase evolution in single-crystalline $LiFePO_4$ followed by in situ scanning X-ray microscopy of a

micrometre-sized battery. *Nat Commun* 2015;6:6045. DOI
7. Merryweather AJ, Schnedermann C, Jacquet Q, Grey CP, Rao A. Operando optical tracking of single-particle ion dynamics in batteries. *Nature* 2021;594:522-8. DOI
8. Xu Z, Hou D, Kautz DJ, et al. Charging reactions promoted by geometrically necessary dislocations in battery materials revealed by in situ single-particle synchrotron measurements. *Adv Mater* 2020;32:2003417. DOI
9. Quinn A, Moutinho H, Usseglio-Viretta F, Verma A, Smith K, et al. Electron backscatter diffraction for investigating lithium-ion electrode particle architectures. *Cell Rep Phys Sci* 2020;1:100137. DOI
10. Xu Y, Hu E, Zhang K, et al. In situ visualization of state-of-charge heterogeneity within a $LiCoO_2$ particle that evolves upon cycling at different rates. *ACS Energy Lett* 2017;2:1240-5. DOI
11. Singer A, Zhang M, Hy S, et al. Nucleation of dislocations and their dynamics in layered oxide cathode materials during battery charging. *Nat Energy* 2018;3:641-47. DOI
12. Martens I, Vostrov N, Mirolo M, et al. Defects and nanostrain gradients control phase transition mechanisms in single crystal high-voltage lithium spinel. *Nat Commun* 2023;14:6975. DOI
13. Cha W, Song S, Jeong NC, et al. Exploration of crystal strains using coherent x-ray diffraction. *New J Phys* 2010;12:035022. DOI
14. Chahine GA, Richard MI, Homs-Regojo RA, et al. Imaging of strain and lattice orientation by quick scanning X-ray microscopy combined with three-dimensional reciprocal space mapping. *J Appl Cryst* 2014;47:762-9. DOI
15. Leake SJ, Favre-Nicolin V, Zatterin E, et al. Coherent nanoscale X-ray probe for crystal interrogation at ID01, ESRF - The European Synchrotron. *Mater Des* 2017;119:470-1. DOI
16. Leake SJ, Chahine GA, Djazouli H, et al. The Nanodiffraction beamline ID01/ESRF: a microscope for imaging strain and structure. *J Synchrotron Radiat* 2019;26:571-84. DOI
17. Martens I, Vanpeene V, Vostrov N, et al. Imaging voids and defects inside Li-ion cathode $LiNi_{0.6}Mn_{0.2}Co_{0.2}O_2$ single crystals. *ACS Appl Mater Interfaces* 2023;15:59319-28. DOI
18. Purushottam Raj Purohit RRP, Tardif S, Castelnau O, et al. LaueNN: neural-network-based *hkl* recognition of Laue spots and its application to polycrystalline materials. *J Appl Cryst* 2022;55:737-50. DOI
19. Rauch EF, Véron M. Automated crystal orientation and phase mapping in TEM. *Mat Charact* 2014;98:1-9. DOI
20. Carnis J, Gao L, Labat S, et al. Towards a quantitative determination of strain in bragg coherent X-ray diffraction imaging: artefacts and sign convention in reconstructions. *Sci Rep* 2019;9:17357. DOI
21. Li J, Hong Y, Yan H, et al. Probing lattice defects in crystalline battery cathode using hard X-ray nanoprobe with data-driven modeling. *Energy Stor Mater* 2022;45:647-55. DOI
22. Liu X, Xu GL, Kolluru VSC, et al. Origin and regulation of oxygen redox instability in high-voltage battery cathodes. *Nat Energy* 2022;7:808-17 DOI
23. Li S, Qian G, He X, et al. Thermal-healing of lattice defects for high-energy single-crystalline battery cathodes. *Nat Commun* 2022;13:704. DOI
24. Zhang SS. Problems and their origins of Ni-rich layered oxide cathode materials. *Energy Stor Mater* 2020;24:247-54. DOI
25. Lin CK, Ren Y, Amine K, Qin Y, Chen Z. In situ high-energy X-ray diffraction to study overcharge abuse of 18650-size lithium-ion battery. *J Power Sources* 2013;230:32-7. DOI
26. Borkiewicz OJ, Wiaderek KM, Chupas PJ, Chapman KW. Best practices for operando battery experiments: influences of X-ray experiment design on observed electrochemical reactivity. *J Phys Chem Lett* 2015;6:2081-5. DOI
27. Corley-Wiciak C, Zoellner MH, Zaitsev I, et al. Lattice deformation at the sub-micron scale: X-ray nanobeam measurements of elastic strain in electron shuttling devices. *Phys Rev Appl* 2023;20:024056. DOI
28. Corley-Wiciak C, Richter C, Zoellner MH, et al. Nanoscale mapping of the 3D strain tensor in a germanium quantum well hosting a functional spin qubit device. *ACS Appl Mater Interfaces* 2023;15:3119-30. DOI
29. Li Y, Zatterin E, Conroy M, et al. Electrostatically driven polarization flop and strain-induced curvature in free-standing ferroelectric superlattices. *Adv Mater* 2022;34:2106826. DOI
30. Mapping the complex evolution of ferroelastic/ferroelectric domain patterns in epitaxially strained $PbTiO_3$ heterostructures. *APL Mater* 2023;11:061126. DOI
31. Zatterin E. id01-sxdm. *Zenodo* 2024. DOI
32. Thomas V, Damien N, Carsten R, Edoardo Z, Ang Z. xsocs. *Zenodo* 2024. DOI
33. Vostrov N, Martens I, Colalongo M, et al. Plastic deformation of $LiNi_{0.5}Mn_{1.5}O_4$ single crystals due to domain orientation dynamics. *ChemRxiv* 2023. DOI
34. Choudhary K, Santos Mendoza IO, Nadeina A, et al. Operando X-ray diffraction in transmission geometry « at home » from tape casted electrodes to all-solid-state battery. *J Power Sources* 2023;553:232270. DOI
35. Wolfman M, May BM, Cabana J. Visualization of electrochemical reactions in battery materials with X-ray microscopy and mapping. *Chem Mater* 2017;29:3347-62. DOI
36. Ulvestad A, Cho HM, Harder R, et al. Nanoscale strain mapping in battery nanostructures. *Appl Phys Lett* 2014;104:073108. DOI
37. Li L, Xie Y, Maxey E, Harder R. Methods for *operando* coherent X-ray diffraction of battery materials at the advanced photon source. *J Synchrotron Radiat* 2019;26:220-9. DOI
38. Robinson IK, Vartanyants IA, Williams GJ, Pfeifer MA, Pitney JA. Reconstruction of the shapes of gold nanocrystals using coherent X-Ray diffraction. *Phys Rev Lett* 2001;87:195505. DOI
39. Pfeifer MA, Williams GJ, Vartanyants IA, Harder R, Robinson IK. Three-dimensional mapping of a deformation field inside a nanocrystal.

*Nature* 2006;442:63-6. DOI
40. Li Y, El Gabaly F, Ferguson TR, et al. Current-induced transition from particle-by-particle to concurrent intercalation in phase-separating battery electrodes. *Nat Mater* 2014;13:1149-56. DOI
41. Dreyer W, Jamnik J, Guhlke C, et al. The thermodynamic origin of hysteresis in insertion batteries. *Nat Mater* 2010;9:448-53. DOI
42. Huang JJ, Weinstock D, Hirsh H, et al. Disorder dynamics in battery nanoparticles during phase transitions revealed by operando single-particle diffraction. *Adv Energy Mater* 2022:12:2103521. DOI
43. Li Y, Li X, Du C, et al. Degradation by kinking in layered cathode materials. *ACS Energy Lett* 2021;6:3960-9. DOI
44. Sharifi-Asl S, Yurkiv V, Gutierrez A, et al. Revealing grain-boundary-induced degradation mechanisms in Li-rich cathode materials. *Nano Lett* 2020;20:1208-17. DOI
45. Lee SY, Park GS, Jung C, et al. Revisiting primary particles in layered lithium transition-metal oxides and their impact on structural degradation. *Adv Sci* 2019;6:1800843. DOI
46. Shen K, Wang Y, Zhang J, et al. Revealing the effect of grain boundary segregation on Li ion transport in polycrystalline anti-perovskite $Li_3ClO$: a phase field study. *Phys Chem Chem Phys* 2020;22:3030-6. DOI
47. Xu Z, Jiang Z, Kuai C, et al. Charge distribution guided by grain crystallographic orientations in polycrystalline battery materials. *Nat Commun* 2020;11:83. DOI
48. Fujii Y, Miura H, Suzuki N, Shoji T, Nakayama N. Structural and electrochemical properties of $LiNi_{1/3}Co_{1/3}Mn_{1/3}O_2$: calcination temperature dependence. *J Power Sources* 2007;171:894-903. DOI
49. Langdon J, Manthiram A. A perspective on single-crystal layered oxide cathodes for lithium-ion batteries. *Energy Stor Mater* 2021;37:143-60. DOI
50. Meng XH, Lin T, Mao H, et al. Kinetic origin of planar gliding in single-crystalline Ni-rich cathodes. *J Am Chem Soc* 2022;144:11338-47. DOI
51. Wang T, Ren K, He M, et al. Synthesis and manipulation of single-crystalline lithium nickel manganese cobalt oxide cathodes: a review of growth mechanism. *Front Chem* 2020;8:00747 DOI
52. Robinson I, Harder R. Coherent X-ray diffraction imaging of strain at the nanoscale. *Nat Mater* 2009;8:291-8. DOI
53. Fienup JR. Phase retrieval algorithms: a personal tour [Invited]. *Appl Opt* 2013;52:45-56. DOI
54. Marchesini S. Publisher's note: "invited article: a unified evaluation of iterative projection algorithms for phase retrieval" [Rev. Sci. Instrum. 78, 011301 (2007)]. *Rev Sci Instrum* 2007;78:049901. DOI